NUCL SCI TECH (2022) 33:147
https://doi.org/10.1007/s41365-022-01124-9

Design, fabrication, and testing of low-group-velocity S-band traveling-wave accelerating structure

Xian-Cai Lin[1,2] · Hao Zha[1,2] · Jia-Ru Shi[1,2] · Liu-Yuan Zhou[1,2] · Yi-Fan Liang[1,2] · Jian Gao[1,2] · Qiang Gao[1,2] · Huai-Bi Chen[1,2] · Chuan-Xiang Tang[1,2]

Received: 29 June 2022 / Revised: 20 September 2022 / Accepted: 21 September 2022 / Published online: 18 November 2022

Abstract To implement the Tsinghua Thomson Scattering X-ray Source upgrade plan and the Very Compact Inverse Compton Scattering Gamma-ray Source (VIGAS) program, a new 1.5-m traveling-wave accelerating structure was designed to replace the old 3-m SLAC-type structure with the aim of increasing the accelerating gradient from 15 to 30 MV/m. The new type of structure works in the $3\pi/4$ mode with a comparatively low group velocity varying from $0.007c$ to $0.003c$ to increase the accelerating gradient at a given power. An elliptical iris was employed to reduce the surface field enhancement. The filling process of the low-group-velocity structure was analyzed using a circuit model. After fabrication, the structure was precisely tuned using the non-contact tuning method, followed by detailed low-power radiofrequency measurements. The structure was first installed and utilized at a beamline for the terahertz experiment at Tsinghua University. After 120 h of conditioning, it is now operating at a gradient of 24.2 MV/m and a 20.7-MW input power, with the klystron operating at its full power. It is expected to generate an accelerating gradient of 30 MV/m when the klystron power is upgraded to 30 MW in the near future.

This work was supported by the National Natural Science Foundation of China (NSFC) (Nos.11922504 and 12027902).

✉ Jia-Ru Shi
shij@mail.tsinghua.edu.cn

[1] Department of Engineering Physics, Tsinghua University, Beijing 100084, China

[2] Key Laboratory of Particle and Radiation Imaging (Tsinghua University), Ministry of Education, Beijing 100084, China

Keywords Traveling-wave accelerating structure · Cavity optimization · Tuning method · High-power test

1 Introduction

The S-band SLAC-type traveling-wave (TW) accelerating structure was first studied and used in the Stanford Two-Mile accelerator [1]. In the 1980s, this type of structure was developed for the injectors of the Large Electron–Positron Collider (LEP) at CERN [2]. In recent decades, because of its stability and high performance, the S-band TW accelerating structure has played an important role in the injectors of coherent light sources and free-electron lasers (FELs), such as the LINAC Coherent Light Source (LCLS) at SLAC [3], Sorgente Pulsata e Amplificata di Radiazione Coerente (SPARC) at the National Institute for Nuclear Physics (INFN) [4], the Swiss FEL at the Paul Scherrer Institute (PSI) [5], and MAX IV at Lund University [6]. In recent years, S-band structures have also been adopted in beam facilities for Thomson scattering X-ray sources [7–9] and medical research [10–12].

The Tsinghua Thomson Scattering X-ray Source (TTX) has been operating with an SLAC-type structure and has served as a tunable monochromatic X-ray source for advanced X-ray imaging experiments over the past few years [7]. Recently, an upgrade was performed to increase the beam energy from 50 to 150 MeV. To achieve this, two X-band accelerating structures [13] were used to increase the electron energy. However, owing to space limitations in the bunker, the currently operating 3-m SLAC-type structure is planned to be replaced with a 1.5-m one with the accelerating gradient increasing from 15 to 30 MV/m. The

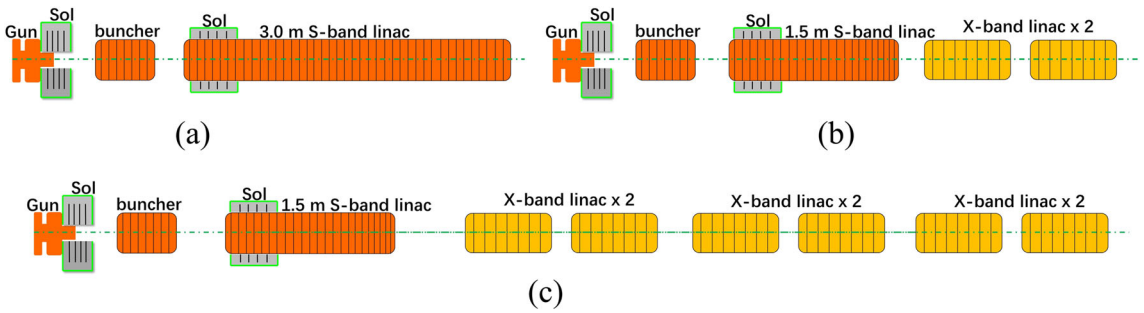

Fig. 1 (Color online) Linac layouts of the **a** present TTX facility, **b** TTX upgrade plan, and **c** VIGAS program

present and proposed linac layouts are shown in Fig. 1a and b, respectively [14].

In 2020, another inverse Compton scattering (ICS) facility for advanced X/γ-ray imaging applications called the Very Compact ICS Gamma-ray Source (VIGAS) was approved at Tsinghua University, which utilizes a similar injector to the TTX upgrade plan. The layout of the accelerator system of the VIGAS facility is shown in Fig. 1c [15].

In the accelerator system of the VIGAS facility, an S-band photocathode electron gun was employed to produce 5-MeV electron bunches [16]. The 1.5-m S-band accelerator was used to boost the energy to 50 MeV and achieve emittance compensation. The injector of the VIGAS program employs the S-band scheme because it can realize a narrow bandwidth of inverse Compton scattered light [15] and the technology is comparatively mature at Tsinghua University. The main accelerating section of this system consists of six X-band, 0.6-m structures, which operate at 80 MV/m and further boost the energy to 350 MeV [17, 18]. Both TTX and VIGAS operate in the single-bunch mode. As an important part of the S-band injector, the 1.5-m S-band accelerator developed in this study will play a key role in ICS experiments and relevant studies at Tsinghua University.

An accelerating structure is a device that converts microwave energy into beam energy. For a TW periodic structure, the accelerating gradient can be calculated as [19]

$$E_{\mathrm{a}} = \sqrt{\omega r P/\left(v_{\mathrm{g}} Q\right)}, \tag{1}$$

where E_{a} represents the accelerating gradient, ω represents the working angular frequency, r represents the shunt impedance per meter, P represents the power flow through the periodic cell, v_{g} represents the group velocity, and Q represents the intrinsic quality factor. Equation (1) indicates that a lower group velocity can convert microwave power to a higher accelerating gradient and achieve the same energy gain at a shorter distance. To motivate the development of compact facilities, the new type of structure is designed to operate at a lower group velocity than previously reported structures, as shown in Table 1. The performance of this low-group-velocity structure was investigated in detail in this study.

This study presents the design, fabrication, and testing of a low-group-velocity S-band TW accelerating structure. The remainder of this paper is organized as follows. In Sect. 2, the radiofrequency (RF) design of the S-band acceleration structure is presented. Additionally, the performance of the structure, such as the filling time and accelerating energy fluctuation, is analyzed. Section 3 introduces the fabrication model, tuning, and low-power RF measurements of the proposed structure. In Sect. 4, a high-power test and beam experiment of the structure are presented. Finally, Sect. 5 concludes the paper.

2 RF design and analysis

The design of the S-band structure was briefly introduced in [14] and [22]. In this section, the design is presented with more details, and the methods used to improve the performance compared with the original structure are described.

The shape and field distribution of a single cell are shown in Fig. 2. Two filets are used to enhance the intrinsic quality factor. This method was first employed in the TW structure of LEP injector linacs (LIL) [2]. A 10.6% increase was obtained in the quality factor with 10- and 12-mm filets compared with the purely cylindrical cell shape. For a TW structure, a higher-quality factor results in less power loss along the beam path and better power flow to the rear section of the structure. Asymmetric filets were adopted for fabrication, which will be explained in the next section. The straight part of the cell was reserved for the fabrication of the tuning device. An elliptical iris was adopted because it can achieve a weaker surface field than a round profile. This is essential in high-gradient applications. In this design, an iris thickness of 5.7 mm with an elliptical ratio of 1.8 was selected [22]. A 15% reduction in

Table 1 Group velocities of different S-band accelerating structures

Structure	Length (m)	Filling time (ns)	Average group velocity, v_g/c
TTX upgrade	1.535	1050	0.49%
SLAC [1]	3.048	830	1.22%
LIL prototype [2]	1.5	272	1.84%
Swiss FEL [5]	4.066	840	1.61%
FERMI FEL [20]	2.920	645	1.51%
KEK prototype [21]	1.899	566	1.12%

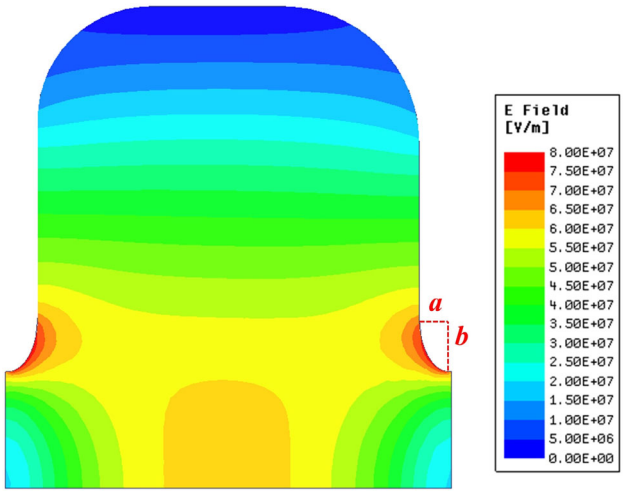

Fig. 2 (Color online) Shape and magnitude of the electric field in a single cell. This cell was simulated with a periodic boundary with a stored energy of 1 J. Here, *a* and *b* represent the short and long axis lengths of the elliptical iris, respectively, and $b/a = 1.8$

the maximum surface field was achieved when adopting this type of elliptical iris compared with the round iris.

Additionally, the phase advance was optimized for a single cell. Different phase advance modes of $2\pi/3$, $3\pi/4$, and $5\pi/6$ were simulated at the same working frequency by adjusting the cell length and outer radius. The simulation results are presented in Table 2. As the phase advance increased, the intrinsic quality factor increased, while the group velocity decreased. The shunt impedance was the highest in the $3\pi/4$ mode; thus, $3\pi/4$ was selected as the working mode.

Table 2 Parameters of the single cells with different phase advances [22]

Parameter	$2\pi/3$	$3\pi/4$	$5\pi/6$
Iris radius (mm)	8.00	8.00	8.00
Q value	15,130	16,438	17,532
Group velocity, v_g/c	0.368%	0.296%	0.208%
Shunt impedance, r (MΩ/m)	70.1	71.6	70.9

According to Eq. (1), a lower group velocity results in a higher gradient with the same input power. Nonetheless, this leads to a longer filling time, smaller iris, and narrower bandwidth. This new type of structure will share the same power source as the photocathode gun, which has a filling time of $\tau_c = 2Q_l/\omega \approx 750$ ns and will be fed with a 1.5-μs pulse. The iris radius of each cell is tapered along the beam path in a constant-gradient structure. The group velocity of each cell should satisfy the relationship introduced in [20]. Through calculations, an iris radius ranging from 10.22 to 8.13 mm was obtained, and the filling time of the whole structure was 1.05 μs.

The input and output couplers were designed to implement power feeding into and out of the structure. A dual-feed scheme was adopted to eliminate the dipole field in the coupler. The optimization of the output and input couplers was performed in Computer Simulation Technology (CST) [23] as introduced in [24]. After the optimization of the coupler, a simulation of the entire structure was performed. The tuning method of [25] was applied to precisely tune the phase advance between the adjacent cells to the design value. The surface field distribution after optimization is shown in Fig. 3. Only the front and rear parts are presented. The maximum surface electric field, which was 10.6 kV/m at an input power of 1 W, was located at the iris of the rear part. The maximum surface magnetic field, which was 29.4 A/m at an input power of 1 W, was located at the output coupler.

Table 3 presents a comparison between the parameters of the S-band low-group-velocity TW structure and those of the original SLAC-type structure. The efficiency of a TW structure is defined as $K = V/P^{1/2}$ [1], where V represents the unloaded accelerating voltage with an input power P. This value indicates the ability to convert the microwave power to the accelerating voltage of a TW structure. Compared with the original SLAC-type structure, the length of the new design was reduced by 49.6%. If we directly reduced the length of the original SLAC-type structure to build a shorter one, the efficiency would have decreased proportionally. However, the efficiency of the new design was only 19.4% lower than that of the original design, because a lower group velocity was adopted in the new design.

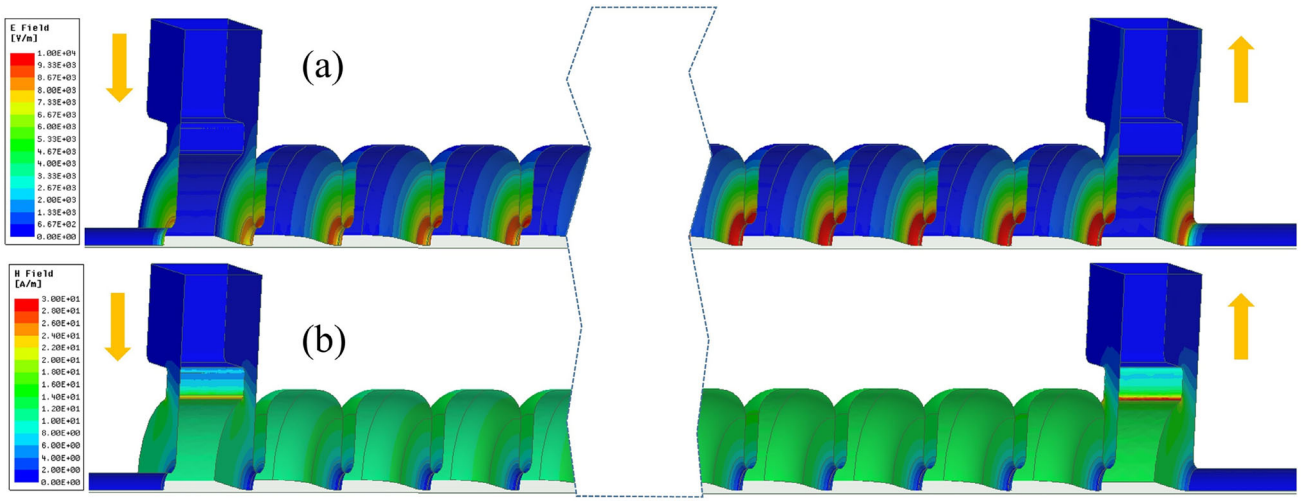

Fig. 3 (Color online) **a** Surface electric field and **b** surface magnetic field distributions of the structure at a 1-W input power. The arrows indicate the power flow

Table 3 Parameters and comparison of the S-band TW structures

Parameter	New design	Original SLAC type
Frequency (GHz)	2.856	2.856
Phase advance per cell	$3\pi/4$	$2\pi/3$
Length (m)	1.535	3.048
Cell numbers	39	86
Iris radius (mm)	10.22–8.13	13.11–9.55
Cell radius (mm)	42.17–42.53	41.73–44.90
Iris thickness (mm)	5.7	5.8
Iris elliptical ratio	1.8	1.3
Filling time (ns)	1050	830
Group velocity, v_g/c	0.302%–0.724%	0.65%–2.04%
Shunt impedance (MΩ/m)	66.2–72.0	53–60
Average gradient @ 30 MW input power (MV/m)	30.9	17.3
Efficiency, $K = V/P^{1/2}$ (MV/(MW)$^{1/2}$)	8.66	10.75

To date, S-band TW structures have not been reported to work with a group velocity as low as $0.00302c$. Therefore, more consideration should be given before fabrication. Two problems influence the performance of the structure. One is the phase stability [26]. The phase stability of a TW structure can be estimated using $\mathrm{d}\varphi/\mathrm{d}f = 2\pi t_{\mathrm{fill}}/n$, where φ represents the phase advance of the periodic cell, t_{fill} represents the filling time, and n represents the number of cells. According to the parameters in Table 3, the phase stabilities of the new and original SLAC designs were 9.7°/MHz and 3.5°/MHz, respectively. In a klystron-powered microwave system, the frequency fluctuation of the structure is mainly caused by the temperature variation of the water-cooling system. According to the linear expansion coefficient factor of copper [27], a 1 °C variation in the cooling water leads to an approximately 50-kHz change in the working frequency of the structure, corresponding to a 0.5° change in the phase advance and only a 4×10^{-5} degradation in the energy gain. This indicates that the phase stability of the new design satisfied the experimental requirements.

The second problem is the filling process of the structure. The filling time of a TW structure is calculated as $t_{\mathrm{fill}} = \sum D_i/v_{\mathrm{g,i}},\ i = 1, 2, \ldots, n$, where D_i and $v_{\mathrm{g,i}}$ represent the cell length and group velocity, respectively, of the ith cell. This algorithm assumes that power flows through a cell with a constant velocity, where the structure is regarded as a non-dispersive device, and hence may be inaccurate for a low-group-velocity structure. From another perspective, the filling process of the structure is an energy storage and release process for each cell, which can be described using the circuit model [28]. The coefficient matrix of the equivalent circuit equation is composed of the RF parameters of the couplers and each cell, as well as the

frequency of the input power [29]. The electric field of each cell, which is proportional to the accelerating voltage, was determined by solving the circuit equation. The spectrum of the electric field of each cell was obtained by sweeping the frequency of the input power. Then, the transient electric field inside each cell and transient average gradient of the entire structure were determined by performing a Fourier transformation with the input signal. Circuit models of the SLAC-type and low-group-velocity structures were analyzed, and the results are shown in Fig. 4. The electric-field spectra of the first, middle, and end cells are shown. The transient average gradient was normalized to 1, whereas the transient field inside a cell was normalized to 0.8. The input signal used for the calculation in Fig. 4b and d had a rising edge of 50 ns and a pulse width of > 3 μs.

As shown in Fig. 4a and c, the bandwidth of the electric field in the low-group-velocity structure was narrower than that in the SLAC-type structure, because the bandwidth is inversely proportional to the group velocity. Figure 4b reveals that the average gradient of the SLAC-type structure reached 97.6% of the steady-state value at the filling-time value of 830 ns, which was calculated using the group velocities of the cells. The average gradient reached a steady state at 910 ns. For the low-group-velocity structure, the average gradient reached 96.3% of the steady-state value at a calculated filling time of 1050 ns. It reached a steady-state value at 1219 ns, as shown in Fig. 4d. Therefore, to fully utilize the accelerating capacity of this low-group-velocity structure, the filling time should be 16% longer than the calculated one. During the operation, the election was injected at 1.5 μs. The trigger-time jitter in the modulator of the klystron was < 10 ns, and the relative beam energy jitter caused by the trigger time and fluctuation of the accelerating gradient from the low-group-velocity structure was 0.05%, as shown in Fig. 4d. Although this value exceeds that of the SLAC-type structure (0.01%), it is negligible in practice.

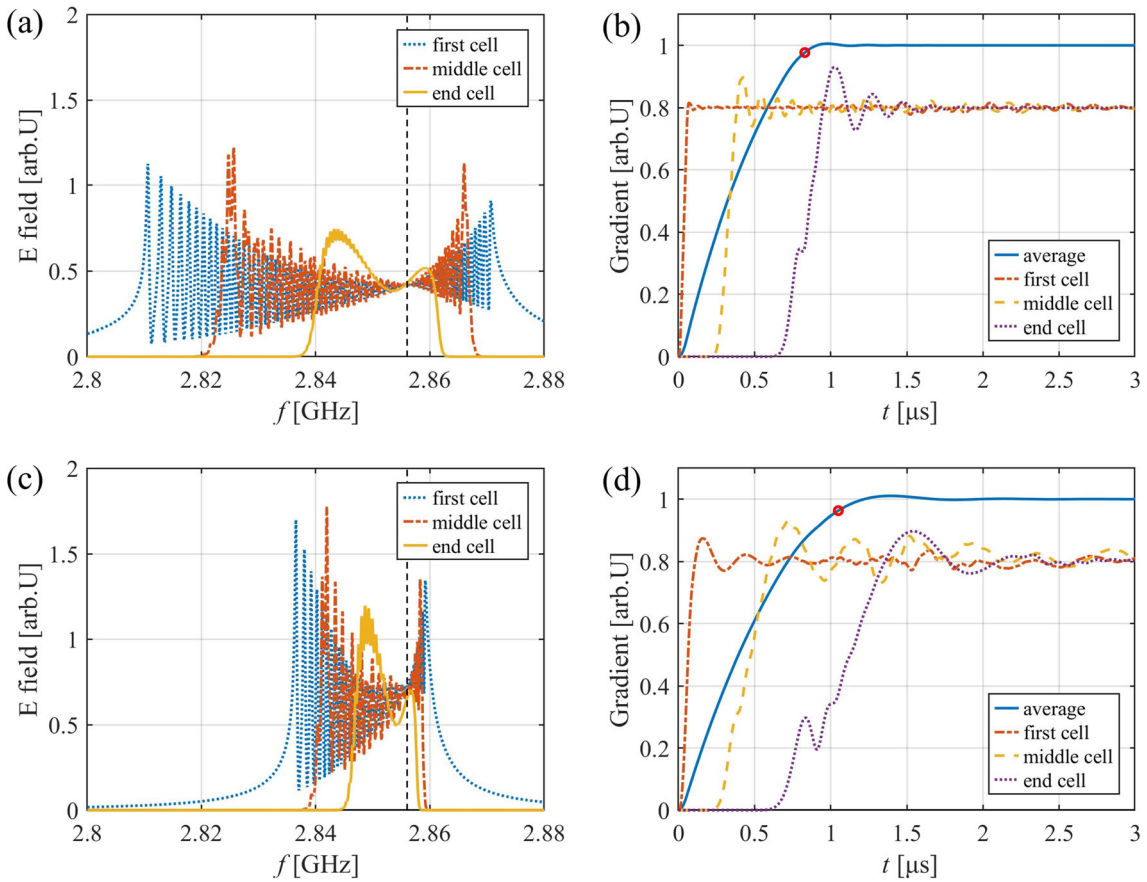

Fig. 4 (Color online) **a** Electric-field spectra of the SLAC-type structure for the first, middle, and end cells of the periodic part; **b** the transient average accelerating gradient of the SLAC-type structure normalized to 1 and transient electric fields in the first, middle, and end cells normalized to 0.8. The red circle indicates the calculated filling time. **c** Electric-field spectra of the low-group-velocity structure in the first, middle, and end cells of the periodic part; **d** the transient average accelerating gradient of the low-group-velocity structure normalized to 1 and transient electric fields in the first, middle, and end cells normalized to 0.8. The red circle indicates the calculated filling time

To validate the circuit model, a series of probes were set in the center of each cell in the CST. The simulated electric-field spectra are shown in Fig. 5. These results are consistent with those obtained from the circuit model. Furthermore, the simulated electric-field spectra of the cells were used to calculate the transient average accelerating gradient using the measured input power waveform.

3 Fabrication, tuning, and low-power RF measurement

The fabrication model of this structure differs from that of the traditional disk-and-loaded structure because of the filets in each cell. A three-dimensional (3D) fabrication model of a single cell is shown in Fig. 6a. Each cavity contained the geometry of a full iris and parts of the cavity cells on both sides. According to the simulation, larger filets resulted in a higher-quality factor. However, the straight part was reserved for fabrication of the tuning holes. Therefore, on the side without the straight part, a larger filet of 12 mm was adopted for a higher-quality factor, whereas on the other side with a straight part, a smaller filet of 10 mm was employed to leave enough length for the straight part. Tuning holes were created on both sides, with the stress areas located in the straight part. Therefore, the pushing and pulling operations on the tuning hole were perpendicular to the structure. The 3D fabrication model of the new type of structure and a photograph of the fabricated structure are shown in Fig. 6b and c, respectively.

After fabrication and brazing, field measurements and tuning were performed on the structure. The low-power RF measurement setup [30] is shown in Fig. 7. The structure was laid horizontally for convenient setup and performing tuning. Two ports of the vector network analyzer (VNA) were connected to the input coupler to avoid assembling the power divider and bend waveguides. The VNA transformed the S-parameters from these two ports into a combined reflection [31]. A bead-pull method based on non-resonant theory [32] was used to measure the field distribution.

The tuning procedure was introduced in [25]. The results of bead-pull field measurements performed before and after tuning are shown in Fig. 8. Owing to the machining errors of the couplers and cells, the electric field in the beam path had a non-uniform distribution, and its polar plot was irregular. After tuning, the errors were compensated, and the measured field distribution was similar to the designed one [14].

The phase advance is defined as the difference between the phases of the next adjacent cell and the selected cell. The phase advances before and after tuning are shown in Fig. 9. In the presence of a standing wave inside the structure, the phase advances oscillated around the operating mode. After tuning, the standing wave inside the structure was almost completely removed, and the phase advance was distributed next to the working mode. There were ripples in the phase-advance plot with a period of four cells, which were caused by the imperfect tuning of the output coupler.

After tuning, the S-parameters were measured. The results are shown in Fig. 10. The reflection from the input coupler at the working frequency was below –35 dB. The bandwidth of the reflection below –30 dB was 0.42 MHz. The transmission loss from the input coupler to the output coupler was –5.5 dB. The filling time was calculated by deriving the transmission angle at the working point [18].

A comparison of the low-power RF measurement results and the simulation results is presented in Table 4. The

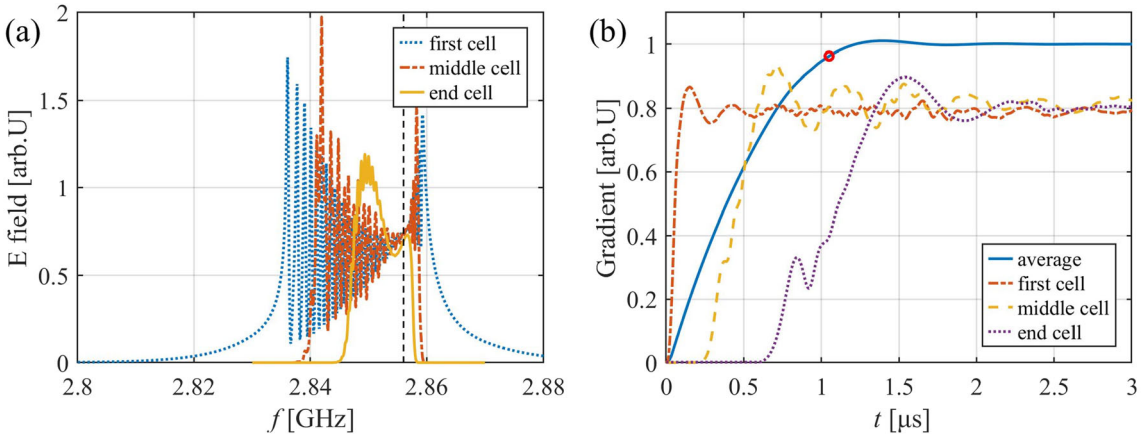

Fig. 5 (Color online) **a** Simulated electric-field spectra of the low-group-velocity structure in the first, middle, and end cells of the periodic part. **b** Transient average accelerating gradient of the low-group-velocity structure normalized to 1 and transient electric fields in the first, middle, and end cells normalized to 0.8

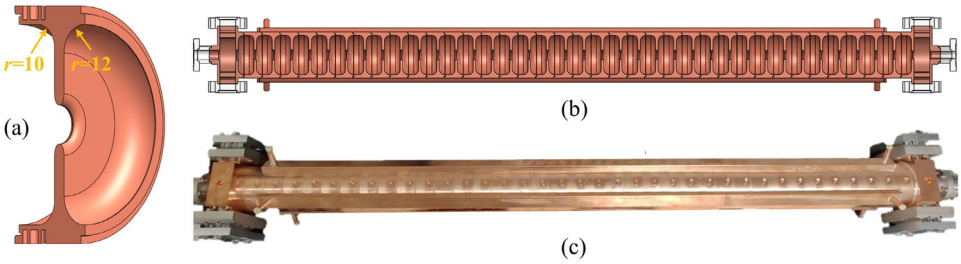

Fig. 6 (Color online) **a** CAD model of a single cell; **b** CAD model of the proposed structure; **c** photograph of the new structure after fabrication

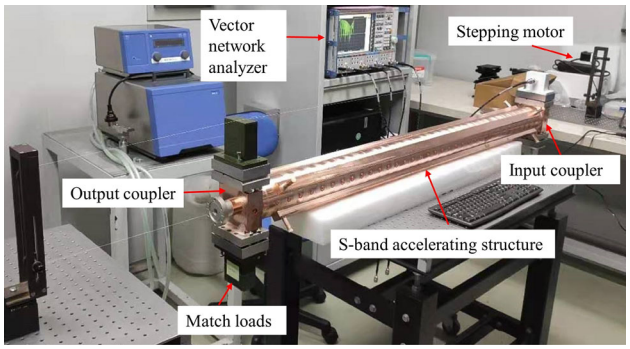

Fig. 7 (Color online) Photograph of the low-power RF measurement setup

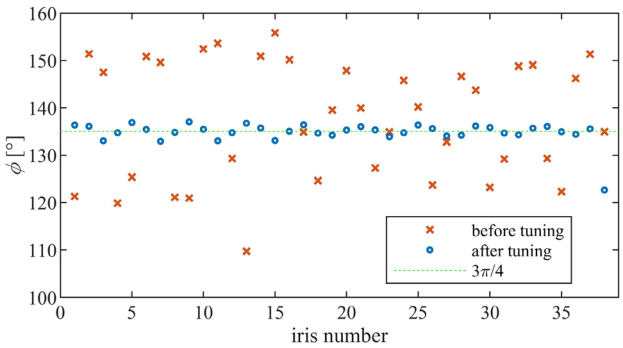

Fig. 9 (Color online) Phase advance between adjacent cells before and after tuning

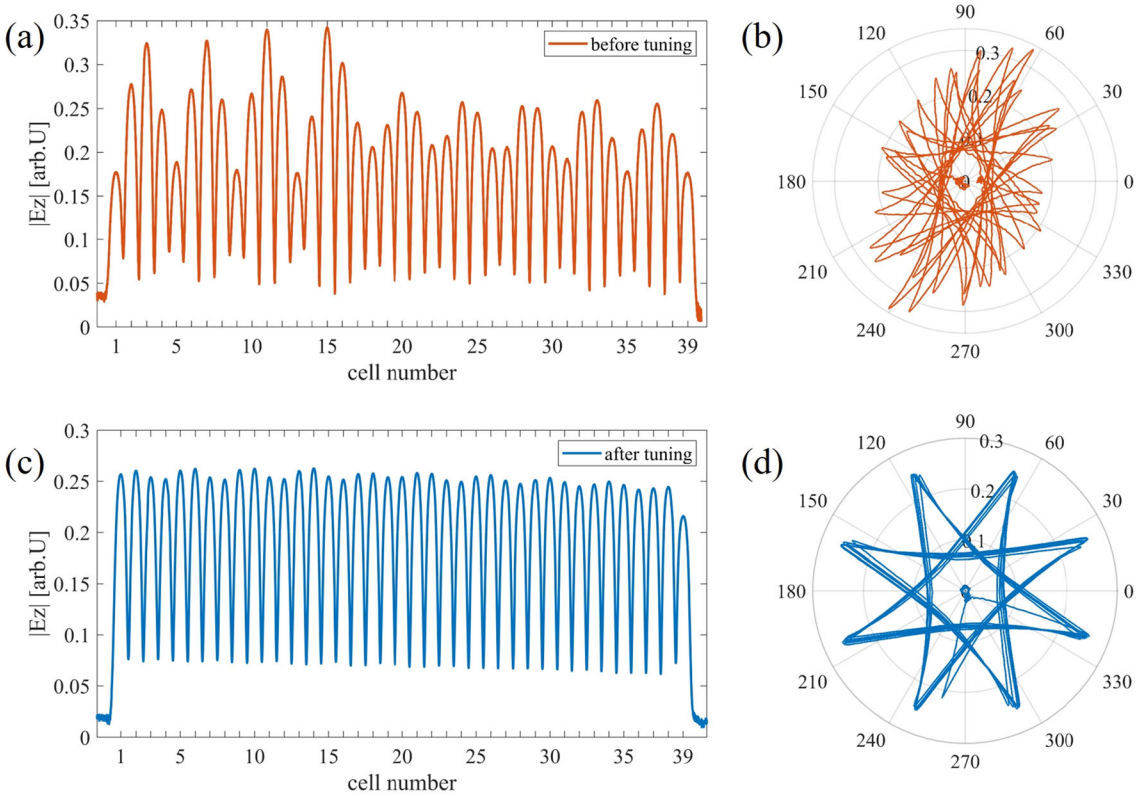

Fig. 8 (Color online) Low-power RF measurement results for the new structure before and after tuning. **a** Relative magnitude of the electric field before tuning; **b** polar plot of the complex electric field before tuning; **c** relative magnitude of the electric field after tuning; **d** polar plot of the complex electric field after tuning

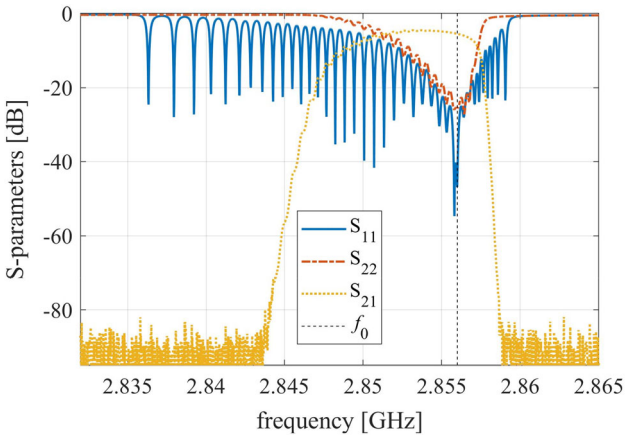

Fig. 10 (Color online) S-parameters of the new structure after tuning. The blue solid line indicates the reflection from the input coupler. The red dash-dotted line indicates the reflection from the output coupler. The yellow dotted line indicates the transmission loss from the input coupler to the output coupler. The black dashed line indicates the working frequency

average phase advance, phase fluctuation, and reflection differed from the simulation values. These parameters can be tuned further to approach the design values. However, the energy degradation caused by these deviations was estimated to be $< 0.1\%$; therefore, no further tuning was applied. The filling time and transmission loss exceeded the design values, indicating that the iris radii of the fabricated cells may have been smaller than the designed ones, resulting in a slightly lower group velocity.

4 High-power test

Owing to the experimental schedule, the new type of structure was first installed at a beamline for the terahertz (THz) experiment at Tsinghua University, which uses the same S-band injector as the TTX upgrade plan, except for the S-band buncher. A photograph of the accelerating structure after installation on the platform is shown in Fig. 11. A power divider and two pairs of 90° H-bend waveguides were installed on the input coupler. Two high-power loads were used to absorb microwaves from the output coupler. A schematic of the RF components and the power feeding system is shown in Fig. 12. An ultraviolet laser was used to drive the photocathode to produce an electron beam, which was accelerated to 5 MeV using an S-band photocathode gun. The energy of the electron beam was increased to approximately 42 MeV using the proposed S-band acceleration structure. A seven-cell defecting cavity was employed to measure the longitudinal distribution of the electron bunches [30]. High-power directional couplers were used to divide the microwaves in each device. A dipole magnet was used to measure the energy of the electron bunches.

After installation at the beamline, the accelerating structure and photocathode gun were simultaneously conditioned. Because no auto-conditioning program was configured on this platform, the conditioning was controlled manually. The breakdown of the accelerating structure and photocathode gun was determined by the rise in the vacuum level, reflection from the accelerating structure, or distortion of the probe signal of the photocathode gun. When the vacuum level exceeded 9×10^{-6} Pa, the microwave system was shut off by the interlock system and restarted until the vacuum was recovered. If both devices were operating without a breakdown for 10 min, the voltage of the modulator was increased by 0.2 kV, which caused an approximately 0.1-MW increment in the output power of the klystron. After 120 h of conditioning at a repetition rate of 10 Hz (4.3×10^6 pulses in total), the voltage of the modulator was increased to saturation. The power waveforms of the structure were measured using directional couplers, coaxial attenuators, crystal detectors, and oscilloscopes. The measured maximum input power for the structure was 22.5 MW, and the mean power was 20.7 MW. The input, reflected, and output waveforms of this structure during the operation are shown in Fig. 13. The simulated electric-field spectra were used to calculate the transient average accelerating gradient along the beam path, as indicated by the green dashed line, which reached the maximum value at the end of the input pulse.

After conditioning, a laser system was used for beam experiments. During the experiments, no breakdown of the new type of structure was observed, and the vacuum level was maintained at 10^{-6} Pa, as measured by a vacuum gauge. The electron energy at the exit of the structure was measured at the end of the beamline using a dipole magnet.

Table 4 Comparison of the low-power RF measurement and simulation results

Parameter	Measured value	Simulation value
Average phase advance (°)	134.8	134.9
Standard deviation of phase advance (°)	2.3	0.7
Reflection S_{11} (dB)	–35	–50
Filling time (ns)	1090	1050
Transmission S_{21} (dB)	–5.5	–5.1

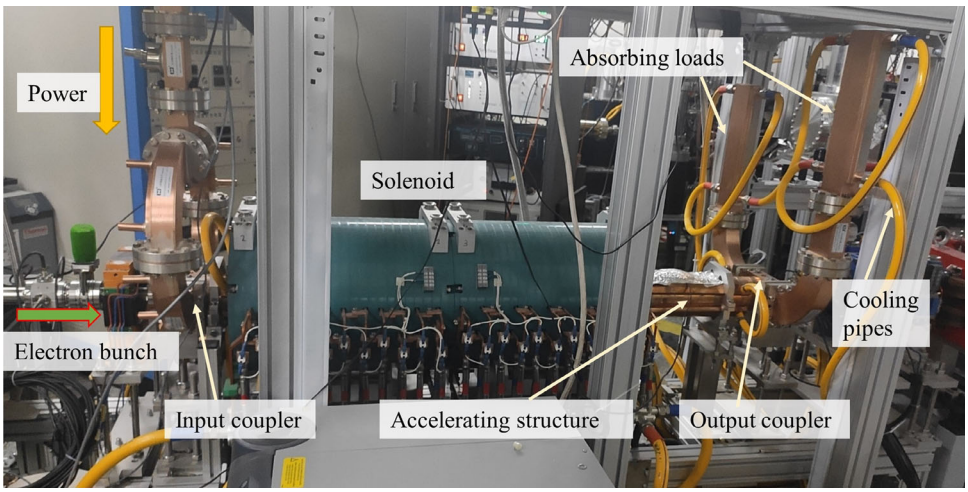

Fig. 11 (Color online) Photograph of the accelerating structure installed on the platform

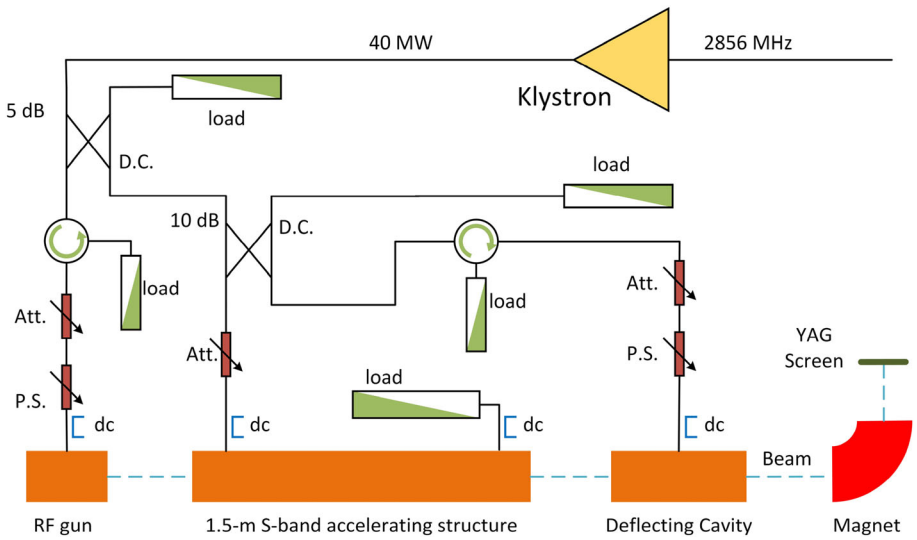

Fig. 12 (Color online) RF components and power feeding system of the THz beamline. Here, "Att." represents the power attenuator, "P.S." represents the phase shifter, "D.C." represents the high-power directional coupler for power dividing, and "dc" represents the directional coupler for power measurement

The parameters of the dipole magnet are presented in Table 5.

Figure 14 shows the output beam profile deflected by the magnet to the yttrium aluminum garnet (YAG) screen, which was collected using a charge-coupled device camera. The energy measured using the dipole magnet was 42.2 MeV. The output energy of the photocathode gun was measured as 5 MeV. Therefore, the beam energy gain from the S-band accelerating structure was 37.2 MeV. Given an effective length of 1.535 m, the measured average accelerating gradient was 24.2 MV/m. The simulated gradient with this input power was 25.7 MV/m, as indicated by the dashed green line in Fig. 13. The measured gradient was 94% of the simulated gradient, which verified the effective acceleration of this structure in the beam experiment. The gradient was lower than the designed one, which is ascribed to the following factors. (1) The output energy of the photocathode gun was measured in the old TTX beamline. In the new beamline, the power from the klystron travels a longer path, resulting in less power to the photocathode. The energy output of the RF gun may have been < 5 MeV, implying that the energy gain may have been larger than the measured value. (2) The structure was preserved in a coarse vacuum conditions for a year before installation, which may have reduced the quality factor.

Owing to the power limit of the microwave system at this THz beamline, the target gradient of 30 MV/m for the TTX upgrade program was not reached. According to the simulation results, the maximum surface electric field at the target gradient was 56 MV/m. Considering the S-band high-gradient test results obtained at KEK [33] and FERMI [20] which reported an accelerating gradient of 40 MV/m with a maximum surface electric field of > 80 MV/m, the target gradient for the TTX upgrade is expected to be achieved in future without reaching the breakdown limit.

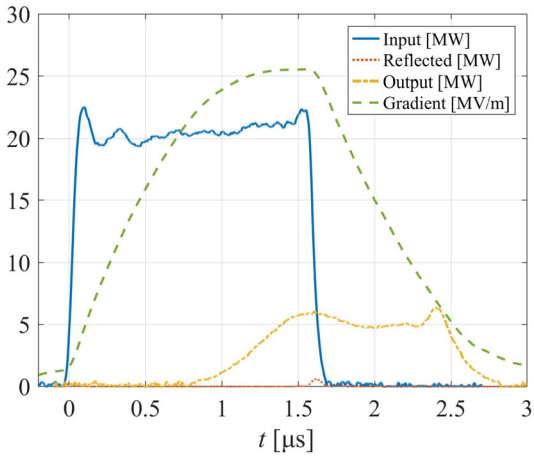

Fig. 13 (Color online) Power waveforms of the new structure in the high-power test. The blue solid line is the input power waveform. The red dotted line is the reflected power waveform. The yellow dash-dotted line is the output power waveform. The green dashed line indicates the transient average gradient calculated using the input power and simulated electric-field spectrum. The electron was injected into the structure at the end of the input pulse

Table 5 Parameters of the analyzing magnet

Parameter	Value
Bending radius (cm)	30
Bending angle (°)	90
Maximum magnetic-field intensity (T)	0.6
Energy range (MeV)	54

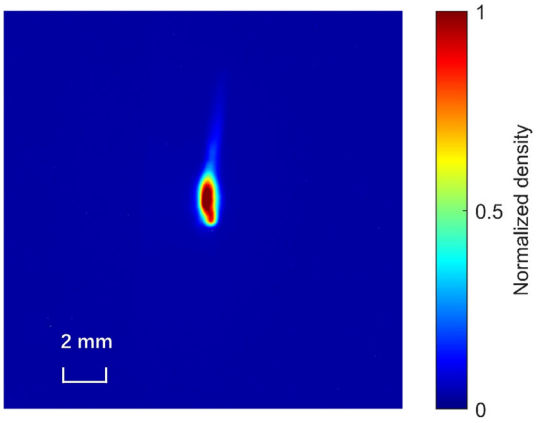

Fig. 14 (Color online) Output beam profile deflected by the dipole magnet

5 Conclusion

A low-group-velocity S-band TW structure was designed at Tsinghua University for the TTX upgrade plan and the VIGAS program. This new structure can increase the accelerating gradient with a given RF power to increase the beam energy to the target parameter in a limited space. The structure was fabricated, tuned, and tested at a high power, and it has been operating at a gradient of 24.2 MV/m with a 20.7-MW input power at the THz beamline at Tsinghua University. The second structure of this type, which is currently under fabrication, will be conditioned with a 30-MW input and reach the target gradient of 30 MV/m in the VIGAS platform in future. In addition to compact ICS and THz sources, this structure can be applied to other high-energy electron research, such as very high-energy electron therapy and neutron generation. The successful operation of this new type of accelerating structure provides reference value for the design of compact high-gradient accelerating structures.

Author contributions All the authors contributed to the conception and design of the study. Material preparation, data collection, and analysis were performed by Xian-Cai Lin, Liu-Yuan Zhou, Qiang Gao, Jian Gao, and Yi-Fan Liang. The first draft of the manuscript was written by Xian-Cai Lin, and all the authors commented on the previous versions of the manuscript. All authors have read and approved the final manuscript.

References

1. R.B. Neal, J.P. Blewett, The Stanford two-mile accelerator. Phys. Today **23**(3), 76–77 (1970). https://doi.org/10.1063/1.3022031
2. G. Bienvenu, J. C. Bourdon, P. Brunet et al., Accelerating Structure Developments for the LEP Injector Linacs (LIL), in *Proceedings of the 1984 Linear Accelerator Conference, Seeheim, Germany* (1984).
3. J. Arthur, P. Anfinrud, P. Audebert et al., Linac Coherent Light Source (LCLS) Conceptual Design Report, 2002. https://doi.org/10.2172/808719
4. D. Alesini, S. Bertolucci, M.E. Biagini et al., The SPARC project: a high-brightness electron beam source at LNF to drive a SASE-FEL experiment. Nucl. Instrum. Methods Phys. Res. Sect. A **507**, 345–349 (2003). https://doi.org/10.1016/S0168-9002(03)00943-4
5. J.-Y. Raguin, The Swiss FEL S-Band Accelerating Structure: RF Design, in *Proceedings of LINAC2012*(2012).
6. S. Thorin, F. Curbis, N. Cutic et al., The MAX IV Linac and first design for an upgrade to 5 Gev to drive an X-ray FEL, in *Proceedings of FEL*(2013).
7. C. Tang, W. Huang, R. Li et al., Tsinghua Thomson scattering X-ray source. Nucl. Instrum. Methods Phys. Res. Sect. A **608**, S70-S74 (2009). doi: https://doi.org/10.1016/j.nima.2009.05.088
8. D. Alesini, M. Bellaveglia, M. E. Biagini et al., Design, realization and test of C-band accelerating structures for the SPARC_LAB linac energy upgrade. Nucl. Instrum. Methods Phys. Res. Sect. A **837**, 161–170 (2016). doi: https://doi.org/10.1016/j.nima.2016.09.010
9. C. Vaccarezza, D. Alesini, M. P. Anania et al., The SPARC_LAB Thomson source. Nucl. Instrum. Methods Phys. Res. Sect. A **829**, 237–242 (2016). doi: https://doi.org/10.1016/j.nima.2016.01.089
10. D. Gamba, R. Corsini, S. Curt et al., The CLEAR user facility at CERN. Nucl. Instrum. Methods Phys. Res. Sect. A **909** (2017), 480–483 (2017). doi: https://doi.org/10.1016/j.nima.2017.11.080

11. Y. Han, F.-G. Angeles, C. Vallerand et al., Optics design and beam dynamics simulation for a VHEE radiobiology beam line at PRAE accelerator. J. Phys. Conference Series **1350**, 012200 (2019). https://doi.org/10.1088/1742-6596/1350/1/012200
12. W.-C. Fang, X.-X. Huang, J.-H. Tan et al., Proton linac-based therapy facility for ultra-high dose rate (FLASH) treatment. Nucl. Sci. Tech. **32**, 34 (2021). https://doi.org/10.1007/s41365-021-00872-4
13. M. Peng, J. Shi, H. Zha et al., Development and high-gradient test of a two-half accelerator structure. Nucl. Sci. Tech. **32**, 60 (2021). https://doi.org/10.1007/s41365-021-00895-x
14. D. Cao, J. Shi, H. Zha et al., Electromagnetic and mechanical design of high gradient S-band accelerator in TTX, in *13th Symposium on Accelerator Physics*(2018).
15. H. Chen, Y. Du, L. Yan et al., Optimization of the compact gamma-ray source based on inverse compton scattering design, in *2018 IEEE Advanced accelerator concepts workshop (AAC)*, IEEE(2018).
16. L. Zheng, Y. Du, Z. Zhang et al., Development of S-band photocathode RF guns at Tsinghua University. Nucl. Instrum. Methods Phys. Res. Sect. A **834,** 98–107 (2016). doi: https://doi.org/10.1016/j.nima.2016.07.015
17. J. Liu, J. Shi, A. Grudiev et al., Analytic RF design of a linear accelerator with a SLED-I type RF pulse compressor. Nucl. Sci. Tech. **31**, 107 (2020). https://doi.org/10.1007/s41365-020-00815-5
18. X.-C. Lin, H. Zha, J.-R. Shi et al., Fabrication, tuning, and high-gradient testing of an X-band traveling-wave accelerating structure for VIGAS. Nucl. Sci. Tech. **33**, 102 (2022). https://doi.org/10.1007/s41365-022-01086-y
19. T. P. Wangler, RF Linear accelerators, John Wiley & Sons, 2008.
20. N. Shafqat, C. Serpico and T. G. Lucas, Design and high-power test of a short prototype of high gradient S-band accelerating structure for the FERMI free electron laser linac upgrade. Nucl. Instrum. Methods Phys. Res. Sect. A **979,** 164473 (2020). doi: https://doi.org/10.1016/j.nima.2020.164473
21. Y. Igarashi, S. Yamaguchi, Y. Higashi et al., High-gradient tests on an S-band accelerating structure, in *Proc. of the 21st International Linac Conference, LINAC2002, Korea*(2002).
22. D. Cao, J. Shi, H. Zha et al., S-band accelerating structure for high-gradient up-grade of TTX, in *Proceedings of IPAC2017*(2017).
23. CST STUDIO SUITE. https://www.cst.com
24. W. Fang, D. Tong, Q. Gu et al., Design and experimental study of a C-band traveling-wave accelerating structure. Chin. Sci. Bull. **56**, 18–23 (2011). https://doi.org/10.1007/s11434-010-4265-2
25. J. Shi, A. Grudiev, W. Wuensch, Tuning of X-band traveling-wave accelerating structures. Nucl. Instrum. Methods Phys. Res. Sect. A **704**, 14–18 (2012). https://doi.org/10.1016/j.nima.2012.11.182
26. X. Huang, Dissertation, Shanghai Institute of Applied Physics, Chinese Academy of Sciences 2017 (in Chinese)
27. J. Shi, Dissertation, Tsinghua University, 2009 (in Chinese)
28. R. M. Jones, V. A. Dolgashev and J. W. Wang, Dispersion and energy compensation in high-gradient linacs for lepton colliders. Phys. Rev. ST - Accelerators and Beams **12**, 051001 (2009). doi: https://doi.org/10.1103/PhysRevSTAB.12.051001
29. J. Shi, S. Zheng, H. Chen, Calculating field distribution of a linear accelerator using equivalent circuit model. High Energy Phys. Nuclear Phys. **30**, 699–703 (2006). https://doi.org/10.1111/j.1745-7254.2006.00260.x
30. X. Lin, H. Zha, J. Shi et al., Development of a seven-cell S-band standing-wave RF-deflecting cavity for Tsinghua Thomson scattering X-ray source. Nucl. Sci. Tech. **32**, 36 (2021). https://doi.org/10.1007/s41365-021-00871-5
31. W. Fan, A. Lu, L. L. Wai et al., Mixed-mode S-parameter characterisation of differential structures, in *Proceedings of the 5th Electronics Packaging Technology Conference (EPTC 2003)*(2003). https://doi.org/10.1109/EPTC.2003.1271579
32. C.W. Steele, A nonresonant perturbation theory. IEEE Trans. Microwave Theory Tech. **14**, 70–74 (1966). https://doi.org/10.1109/TMTT.1966.1126168
33. Y. Igarashi, S. Yamaguchi, Y. Higashi et al., High-gradient tests on S-band 2m-long accelerating structures for KEKB injector linac. in *Particle Accelerator Conference*(2003). https://doi.org/10.1109/PAC.2003.1289738